Modeling the Effect of Wave–Current Interaction on the Three-Dimensional Wind-Driven Circulation of the Eastern Irish Sea

ALAN M. DAVIES

Proudman Oceanographic Laboratory, Bidston Observatory, Birkenhead, Merseyside, England

JOHN LAWRENCE

MAFF Fisheries Laboratory, Pakefield Road, Lowestoft, Suffolk, England

(Manuscript received 29 September 1992, in final form 2 December 1993)

ABSTRACT

A high-resolution (0.5′ north–south by 1.0′ west–east) three-dimensional hydrodynamic model of the eastern Irish Sea is used to examine the influence of enhanced bed friction due to wind–wave effects upon the three-dimensional, wind-induced circulation of the eastern Irish Sea.

The model uses a mixed finite difference–modal approach, in which a standard finite-difference grid is employed in the horizontal, with the Galerkin method, with an expansion of functions (modes) in the vertical, giving a continuous current profile from sea surface to seabed. Vertical eddy viscosity within the model is a function of the flow field.

The model is used to examine the wind-induced response of the area to spatially uniform and constant in time northerly and westerly wind stresses of 1 N m^{-2}. The effect upon bed stresses, and hence the three-dimensional circulation of the region of enhanced bed turbulence due to wind wave effects, is also considered using idealized wave fields. Changes in bed stress, particularly in shallow water regions, have a significant influence upon the wind-induced circulation, especially the wind-induced, near-bed currents.

In addition to calculations using a uniform drag coefficient and bed type, the wind-induced circulation using a range of bed types corresponding to the bed composition, from mud to gravel, of the eastern Irish Sea is also considered. The intensity of near-bed turbulence, and hence drag coefficient, due to wave–current interaction is found to vary significantly with bed type, and this also influences the near-bed currents.

1. Introduction

With the development of new instruments (Green et al. 1990; Lohrmann et al. 1990) capable of measuring enhancements of bed stress due to wind wave activity (Signell et al. 1990; Christoffersen and Jonsson 1985; Grant and Madsen 1979; Grant et al. 1984) and current profiles in the near-bed region, there has been increased interest in developing three-dimensional models that can resolve the near-bed region and take account of enhancements in near-bed turbulence due to wind–wave activity.

To date the majority of this work has involved the use of single point models, the most sophisticated of which use a turbulence energy closure method and resolve the wind–wave period (A. G. Davies 1990, 1991; A. G. Davies et al. 1988; A. M. Davies and Jones 1990). These models clearly show enhanced levels of turbulence at the bed, associated with the high shear wave boundary layer, and the retarding force that this exerts on the flow field. Obviously the computational overhead associated with resolving the wave period and the turbulence energy scheme make it impractical to use these techniques in full three-dimensional calculations. A range of alternative methods based upon eddy viscosity closure exist in the literature (e.g., Signell et al. 1990; Grant and Madsen 1979; Christoffersen and Jonsson 1985), which can also reproduce the enhancement of bed friction and turbulence due to wave–current interaction over a rough bed. Since these methods are computationally inexpensive compared to the turbulence energy approach, they can be readily included in a full three-dimensional, time-dependent hydrodynamic model (Spaulding and Isaji 1987). Recently Signell et al. (1990) included wave–current interaction effects in an idealized estuarine model and showed that it could influence the flow field.

In this paper we use a similar approach to examine the influence of enhancements in bed stress due to wave–current interaction upon the wind-induced circulation of the eastern Irish Sea. Since this effect is known to be important in near-coastal regions, we use a high-resolution grid (Fig. 1) (0.5′ north–south by 1.0′ west–east, approximately a 1-km grid). The model

Corresponding author address: Dr. Alan M. Davies, Proudman Oceanographic Laboratory, Bidston Observatory, Birkenhead, Merseyside L43 7RA, United Kingdom.

uses a standard, regular finite-difference grid in the horizontal.

The model has been used previously (Aldridge and Davies 1993) to determine the M_2 tidal elevation and current in the region, and hence an accurate M_2 tidal input is available to use along the model's open boundary. Since tidal currents are strong in the region (of order, up to 100 cm s^{-1}), it is important to include tidal effects with wind stress forcing in order to obtain the correct levels of turbulence and bed stress in the region. The tidal currents are, however, removed in order to study the influence of wave–current interaction on the wind-driven residual flow.

Initial calculations use a constant bed roughness with uniform northerly and westerly winds and a range of significant wave heights and periods, although subsequently the influence of a spatially variable bed roughness (reflecting the range of bed composition from mud to gravel, Fig. 2) found in the eastern Irish Sea is used. The importance of bed composition and wave–current interaction in determining sediment transport mechanisms has recently been reviewed by Huntley and Bowen (1990) and A. G. Davies (1990).

2. Hydrodynamic model

a. Governing equations

The three-dimensional hydrodynamic equations in polar coordinates are given by

$$\frac{\partial \zeta}{\partial t} + \frac{1}{R\cos\phi}\frac{\partial}{\partial \phi}\int_{-\zeta}^{h} v\cos\phi dz + \frac{1}{R\cos\phi}\frac{\partial}{\partial \chi}\int_{-\zeta}^{h} u dz = 0 \quad (1)$$

$$\frac{\partial u}{\partial t} + \frac{u}{R\cos\phi}\frac{\partial u}{\partial \chi} + \frac{v}{R}\frac{\partial u}{\partial \phi} + w\frac{\partial u}{\partial z} - \frac{uv\tan\phi}{R} - 2\omega\sin\phi v = -\frac{g}{R\cos\phi}\frac{\partial \zeta}{\partial \chi} + \frac{\partial}{\partial z}\left(\mu\frac{\partial u}{\partial z}\right) \quad (2)$$

$$\frac{\partial v}{\partial t} + \frac{u}{R\cos\phi}\frac{\partial v}{\partial \chi} + \frac{v}{R}\frac{\partial v}{\partial \phi} + w\frac{\partial v}{\partial z} + \frac{u^2\tan\phi}{R} + 2\omega\sin\phi u = -\frac{g}{R}\frac{\partial \zeta}{\partial \phi} + \frac{\partial}{\partial z}\left(\mu\frac{\partial v}{\partial z}\right) \quad (3)$$

$$w = \frac{1}{R\cos\phi}\frac{\partial}{\partial \chi}\int_{z}^{h} u dz - \frac{\tan\phi}{R}\int_{z}^{h} v dz + \frac{1}{R}\frac{\partial}{\partial \phi}\int_{z}^{h} v dz. \quad (4)$$

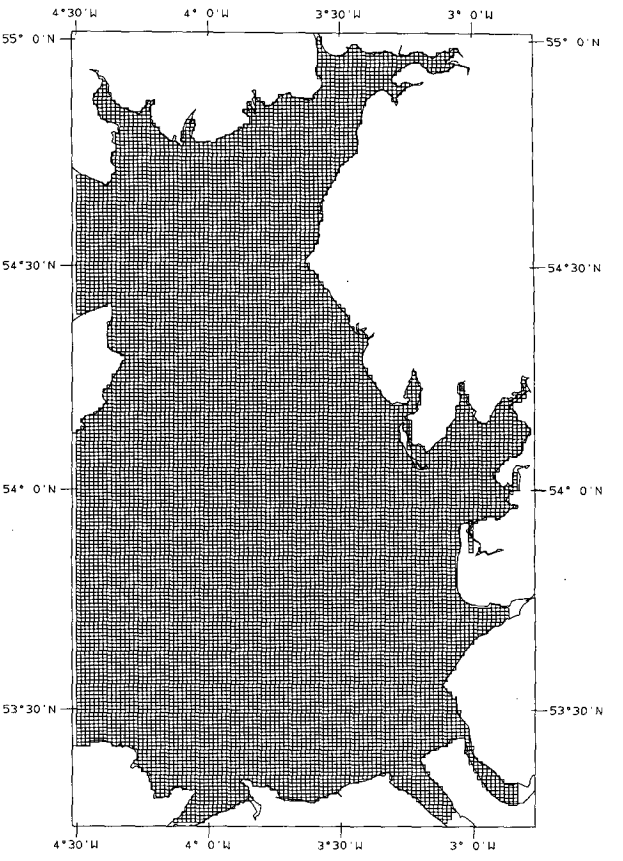

FIG. 1. Finite-difference grid of the three-dimensional eastern Irish Sea model.

In these equations we have neglected the horizontal viscous terms, which are small and can readily be neglected on a fine grid (Oey et al. 1985; James 1990). In these equations χ, ϕ are longitude and latitude with z the depth below the undisturbed surface, h the water depth, and ζ the elevation of the sea surface; t time and R radius of earth; u, v, and w are eastward, northward, and vertical components of velocity; ω the speed of earth's rotation; g acceleration due to gravity; and μ vertical eddy viscosity.

b. Lateral boundary conditions

Along open boundaries, the normal component of current is set to zero for all time. The drying condition of Flather and Heaps (1975) (see also Flather and Hubbert 1990) is used in the model to allow for drying in near-coastal regions in response to tidal and wind forcing.

Along open boundaries a radiation condition, namely,

$$q = q_T + q_m + \frac{C}{h}(\zeta - \zeta_T - \zeta_m), \quad (5)$$

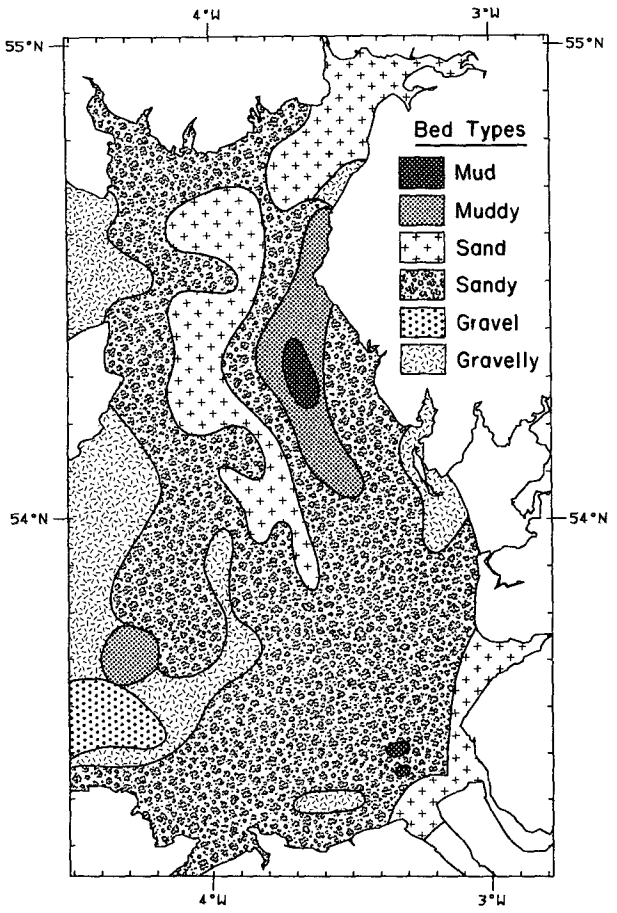

FIG. 2. Schematic showing the spatial variation of bed types.

was applied, with q the normal component of the depth mean current, $C = (gh)^{1/2}$, and

$$q_T = Q_{M_2} \cos(\omega_{M_2} t - \gamma_{M_2}) \quad (6)$$

$$\zeta_T = H_{M_2} \cos(\omega_{M_2} t - G_{M_2}). \quad (7)$$

In Eqs. (6) and (7) ω_{M_2} denotes the speed of the M_2 tidal constituent with H_{M_2} and G_{M_2} the amplitude and phase of tidal elevation; Q_{M_2} and γ_{M_2} are the tidal current. Identical input to that of Aldridge and Davies (1993) was used in the model. The meteorological terms q_m and ζ_m can take account of far-field meteorological forcing upon the eastern Irish Sea due to open boundary effects. As we are concerned here with only the local response, these terms were set to zero.

c. *Surface and bed boundary conditions*

For wind-driven flow, the surface stress is set to the externally specified orthogonal components of the wind stress, namely F_s, G_s; thus,

$$-\rho\left(\mu \frac{\partial u}{\partial z}\right)_{-\zeta} = F_s, \quad -\rho\left(\mu \frac{\partial v}{\partial z}\right)_{-\zeta} = G_s. \quad (8)$$

At the seabed, in the absence of wind waves, the bed-stress components F_B and G_B can be related to the near-bed currents U_h, V_h using a quadratic friction law; thus,

$$F_B = k\rho U_h (U_h^2 + V_h^2)^{1/2} = \tfrac{1}{2} f_c \rho U_h (U_h^2 + V_h^2)^{1/2} \quad (9a)$$

$$G_B = k\rho V_h (U_h^2 + V_h^2)^{1/2} = \tfrac{1}{2} f_c \rho V_h (U_h^2 + V_h^2)^{1/2}. \quad (9b)$$

In Eqs. (9a) and (9b), using oceanographic nomenclature, k is a coefficient of bottom friction, relating bed stress to the current at a reference height, usually 1 m above the seabed (then normally written as C_{100}, the drag coefficient related to currents 100 cm above the seabed). In general, C_{100} will be a spatially varying coefficient depending upon bed types and forms (Heathershaw 1981). In coastal engineering, the factor $f_c = 2k$, termed a "current friction factor," is normally employed.

In the presence of wind wave effects, as we will show later, the factor f_c (and hence k) is increased to take account of increased turbulence due to wave effects enhancing the bed stress.

d. *Numerical solution*

Since extensive details of the numerical approach have been given in the literature (Davies 1983, 1986, 1987, 1992; Davies and Aldridge 1992; Aldridge and Davies 1993), only a very brief indication of the method will be presented here.

To accurately resolve variations in bottom topography, a normalized sigma coordinate is used in the vertical; thus,

$$\sigma = (z + \zeta)/(h + \zeta). \quad (10)$$

The numerical solution proceeds by first transforming the hydrodynamic equations to sigma coordinates and then discretizing using a standard finite-difference grid in the horizontal (Fig. 1) and the Galerkin approach with a modal expansion in the vertical (for example, Davies 1986; Furnes 1983; Gordon and Spaulding 1987). The rate of convergence of the modal expansion can be enhanced by using a mixed basis set (A. M. Davies 1992) and computational efficiency improved by using a time splitting approach (Davies 1987; Aldridge and Davies 1993). The solution method of Davies and Aldridge (1992) was used to ensure stability in shallow water even with a long time step.

The principal advantage of the Galerkin method in the vertical is that it yields a continuous current profile and can accurately resolve boundary layers (A. M. Davies 1992). Also, the method can be readily coded to give highly parallel and vectorized code for the new

generation of multiprocessor vector computers (Davies et al. 1991; 1992).

3. Wave–current interaction model

The wave–current interaction model of Grant and Madsen (1979), in the form applied by Signell et al. (1990) for computational economy, was used in the three-dimensional model to account for increases in the wave friction coefficient f_c due to wave effects. Only a brief description of this model will be presented here, as a detailed discussion with appropriate references can be found in Signell et al. (1990).

The effect of enhanced bed turbulence due to wind wave activity influences the three-dimensional, wind-driven flow field computed by the hydrodynamic model by an increase in the current friction factor f_c and hence the bed stress in the three-dimensional model, when wave effects are present.

Following Signell et al. (1990), we outline the major steps in the formulation of the wave–current interaction model for colinear flow. For simplicity, we use only colinear waves and currents in the calculations described later because we are only interested in the zero-order effect of waves on the circulation, although the method can be applied for waves and currents at an arbitrary angle (Grant and Madsen 1979). The extension to waves and currents at an arbitrary angle is not complicated, but since the wind-induced flow in the model is driven by an idealized uniform constant wind field, the equally idealized assumption of colinear waves and currents is consistent.

For a colinear flow, the total bed shear stress τ_T based upon an instantaneous current shear stress τ_T and maximum wave bed stress τ_w is given by

$$\tau_T = \tau_c + \tau_w \tag{11}$$

with

$$\tau_w = \frac{1}{2} f_w \rho U_w^2, \tag{12}$$

where U_w is the maximum wave orbital velocity outside the wave boundary layer and f_w is the wave friction factor.

The near-bottom wave orbital velocity is given by

$$U_w = \frac{a_w \omega}{\sinh kh} \tag{13}$$

with a_w wave amplitude, ω wave frequency, k wavenumber determined from the linear dispersion relation, and

$$\omega^2 = (gk)\tanh(kh) \tag{14}$$

with g acceleration due to gravity.

The wave friction factor f_w depends upon bed roughness $k_b = 30\ z_o$, where z_o is the roughness length and the near-bottom excursion amplitude $A_b = U_w/\omega$.

Values of f_w can be readily computed from the semiempirical expression (Jonsson 1967; Jonsson and Carlsen 1976, based upon laboratory observations): namely,

$$\frac{1}{4\sqrt{f_w}} + \log_{10}\left(\frac{1}{4\sqrt{f_w}}\right) = -0.08 + \log_{10}\left(\frac{A_b}{k_b}\right). \tag{15}$$

Laboratory measurements and Eq. (15) show that f_w decreases as relative roughness (A_b/k_b) increases.

Following Signell et al. (1990), we assume here that the current does not influence the wave field. (This is a consistent assumption with the method adopted here in which the three-dimensional model is run with the wave field supplied externally, and hence, there is no dynamic feedback from the current model.) The current bed stress, τ_c however, is significantly influenced by the wave field and the time-evolving viscosity field and, hence, depends upon the dynamics of the flow through both the velocity field and the current friction factor f_c.

The calculation of an effective drag coefficient f_c taking into account wave effects was determined as follows. Since the present model assumes that the current does not influence the wave field, then the wave-friction velocity

$$U_{*w} = \left(\frac{\tau_w}{\rho}\right)^{1/2} \tag{16}$$

is readily computed with τ_w given by (12) and f_w taken from (15).

At time $t = 0$, an initial current friction factor f_c, not accounting for waves, was computed from

$$f_c = 2\left[\frac{K}{\ln(30 z_r/k_{bc})}\right]^2 \tag{17}$$

with k_{bc} taken as the Nikuradse roughness $k_b = 30\ z_o$, $K(=0.4)$, von Kármán's constant, and z_r, the reference height at which the slip condition is applied, here taken as 100 cm above the seabed; hence, $f_c = 2k = 2C_{100}$ [Eq. (9a,b)].

Having determined f_c, the current friction velocity U_{*c} can be readily computed from

$$U_{*c} = \left(\frac{\tau_c}{\rho}\right)^{1/2}, \tag{18}$$

with τ_c the vector sum of F_B, G_B from Eqs. (9a,b).

The combined friction velocity U_{*cw} for waves and currents is given by

$$U_{*cw} = (U_{*c}^2 + U_{*w}^2)^{1/2}. \tag{19}$$

The apparent bottom roughness k_{bc} felt by the current due to the presence of the waves is given by

$$k_{bc} = k_b\left[C_1 \frac{U_{*cw}}{U_w}\frac{A_b}{k_b}\right]^{\beta} \tag{20}$$

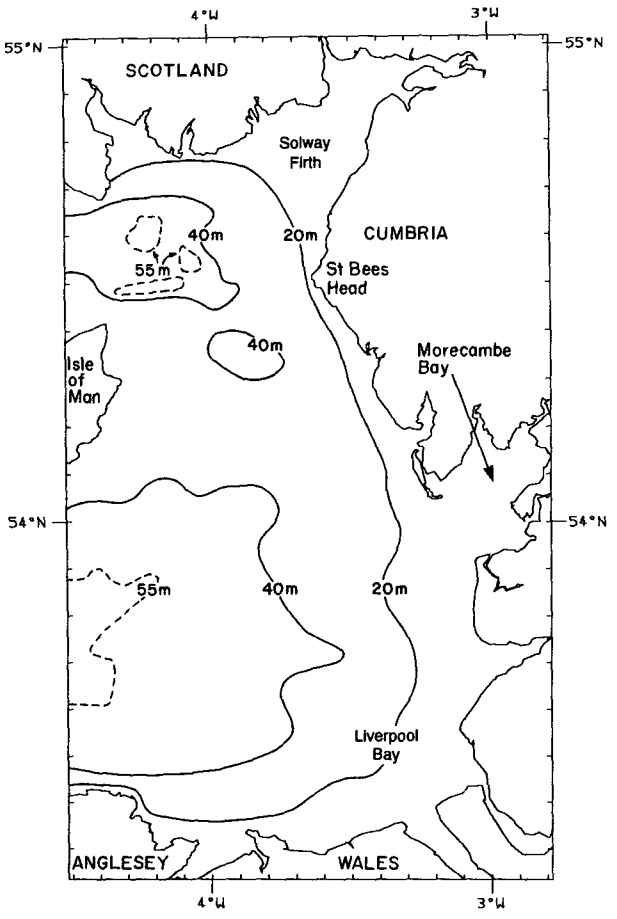

FIG. 3. Contours of the bottom topography of the eastern Irish Sea (all depths in meters).

with

$$\beta = 1 - \frac{U_{*c}}{U_{*cw}} \tag{21}$$

and

$$C_1 = 24.0. \tag{22}$$

This value of k_{bc} is then used at the next time step to determine f_c, and hence, the bed stress in the three-dimensional model, using Eqs. (9a,b).

4. Computed wind-induced circulation

a. Numerical model

The model uses polar coordinates on the finite-difference grid, shown in Fig. 1, which has a resolution of 0.5′ north–south, 1.0′ west–east. The bottom topography of the region is characterized by water depths of the order of 50 m (Fig. 3) in the region of the model's open boundary, which extends north and south from the Isle of Man. The shallow area (water depths of order 30 m) to the east of the Isle of Man is separated from the shallow near-coastal band (water depths below 20 m) by a deeper region (water depths exceeding 40 m), as shown in Fig. 3.

A range of bed types from mud to gravel occur in the region (Fig. 2). Since the wind wave orbital velocity decreases rapidly with depth below the sea surface and with wave period (Table 1), enhancements in bed stress due to short-period wind waves (periods below 6 sec) will occur only in the nearshore region. For this reason, it is essential to use the fine grid shown in Fig. 1 in order to resolve this area. {Table 1, gives the wave orbital velocity for a unit wave amplitude; however, since orbital velocity is proportional to amplitude [Eq. (13)], results can be easily scaled.} Also, since the magnitude of wave–current interaction depends upon bed roughness, it is necessary to examine how the wind-driven current is modified not only by the presence of wave–current interaction but also by spatial variations in the bed roughness.

In the series of calculations described later, the model was forced by a suddenly imposed and spatially uniform wind stress of 1.0 N m^{-2}, corresponding to either a uniform westerly or northerly wind. Wind stresses of this order occur during extreme winter storm conditions [see, for example, the storm simulation of Davies and Jones (1992)]. Depending upon wind direction, duration, and intensity, a range of significant wave heights and periods can be generated during these storms (Carter 1982), although wave amplitudes and periods of the order of 0.5–1.5 m and 6–10 sec can occur during storms (Draper 1992). Initial conditions of zero elevation and motion were taken in all cases. Meteorological input ζ_m and q_m along the open boundary was set to zero. However, to obtain the correct background level of turbulence and bed stress, M_2 tidal forcing, identical to that used by Aldridge and Davies (1993), was applied along the open boundary.

Based upon Irish Sea observations (Bowden et al. 1959), eddy viscosity in the model was parameterized using

$$\mu = K(\bar{u}^2 + \bar{v}^2)^{1/2}h,$$

with $K = 0.0025$ and $\bar{u}$, $\bar{v}$ the depth-mean current. This parameterization of viscosity is identical to that

TABLE 1. Values of bed wave orbital velocity U_0 (cm s^{-1}) for a wave amplitude of 1.0 m in a range of water depths (h) computed with two wave periods: (a) T_M = 10.0 s and (b) T_M = 6.0 s.

Period (sec)	h (m)				
	10	20	30	40	50
10	85	51	34	23	16
6	62	22	7	2	1

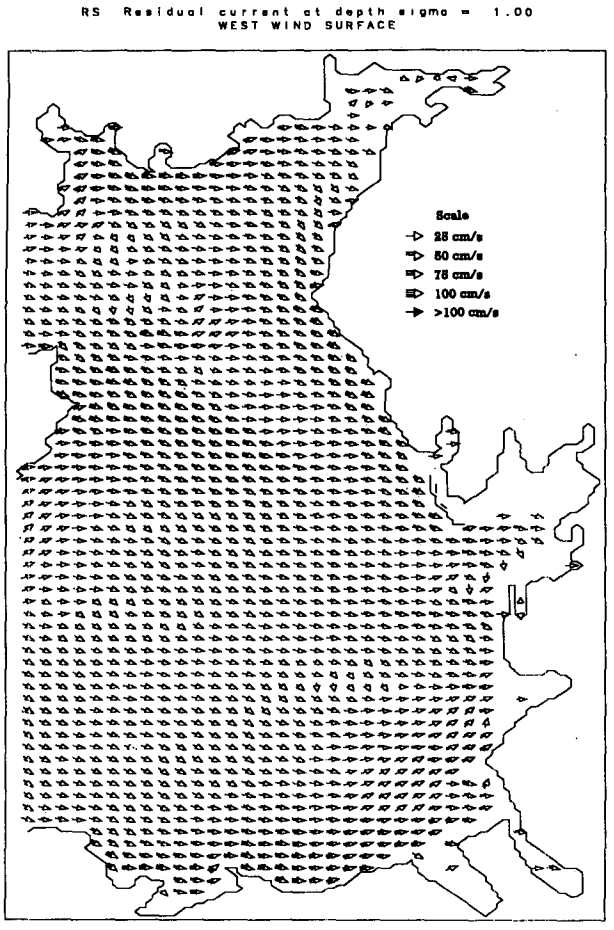

FIG. 4a. Computed surface currents at every third grid point of the model induced by a uniform westerly wind stress of 1 N m^{-2}.

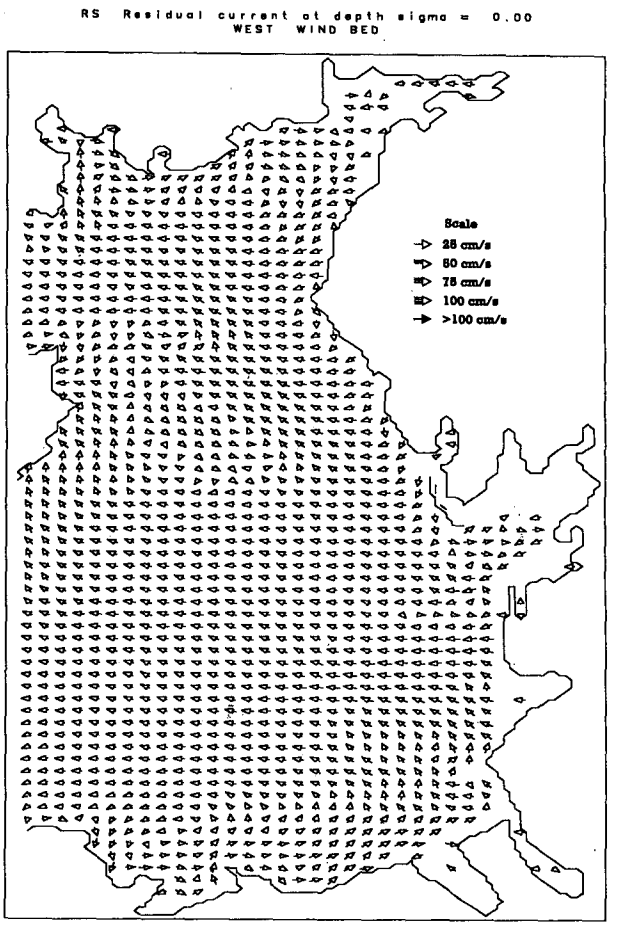

FIG. 4b. As in (a) but for bed currents.

used by Aldridge and Davies (1993) in a three-dimensional model of the M_2 tide in this region.

A time splitting algorithm (Davies 1987; Aldridge and Davies 1993) was used to integrate the equations in time, with the gravity wave term requiring a time step of 25 sec, although the vertical diffusion term could be integrated with a time step 24 times longer than this. After four tidal cycles, the effect of the initial conditions had been removed, and a steady wind-driven flow superimposed upon a periodic tidal regime had been obtained.

In an initial series of calculations, the wind-driven residual was obtained by running the model with the tide alone for an equivalent period of time and subtracting this flow from that with the tide and wind. In subsequent calculations, however, particularly those involving wave–current interaction, this method failed to remove the tidal current from the wind-driven current, particularly in shallow water regions. The primary reason for this was that in the calculation with tidal plus meteorological forcing and wind wave effects included, the resulting wave–current interaction modified the bottom friction coefficient, which influenced tidal currents, particularly near-bed currents. Another reason is that even in the absence of wind wave effects, the nonlinear frictional terms in the model due to both bottom friction and eddy viscosity produce enhanced levels of friction when there is a wind-driven flow superimposed upon a tidal flow. Since these terms are nonlinear, the tidal current is modified in a nonlinear manner by the presence of the wind-induced flow, and it is no longer possible to extract the wind-driven flow by subtracting a tide-only solution. For these reasons, the residual flow fields were obtained by running the model for five tidal cycles and harmonically analyzing the final cycle to give the residual flow. This velocity field is primarily the meteorologically induced flow (currents of order 50 cm s^{-1}) with a small tidal residual [typically less than 5 cm s^{-1}; Aldridge and Davies (1993)] due to the nonlinearity in the hydrodynamic equations. Since the tidal residual current could be readily obtained from a harmonic analysis of a tide-only run of the model, this could be removed to yield a meteorologically induced circulation.

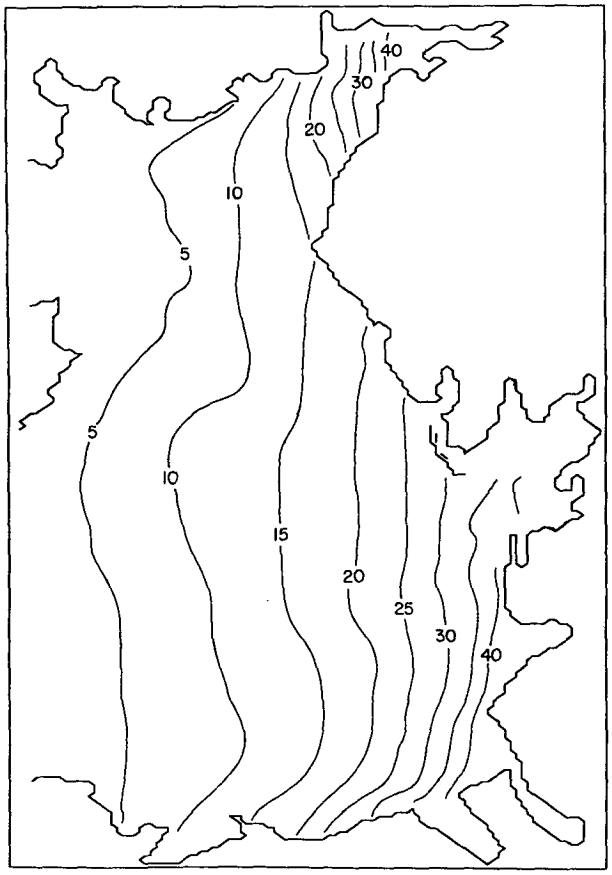

FIG. 4c. Computed residual sea surface elevation (cm) induced by a uniform westerly wind stress of 1 N m^{-2}.

b. *Wind-induced circulation due to uniform westerly and northerly winds of 1 N m^{-2}*

In an initial series of calculations a constant bottom friction coefficient $k = 3.75 \times 10^{-3}$ [a value found by Aldridge and Davies (1993) to yield an optimal M_2 tidal distribution in the area and to correspond to the average k value based upon bed types (Fig. 2)] was used. Surface and bed meteorologically induced currents computed with this k value, and uniform westerly and northerly wind stresses of 1 N m^{-2} with no wave effects, are shown in Figs. 4a,b and Figs. 5a,b.

Surface currents plotted at every third grid point of the model (Fig. 4a) show a direct wind-driven, essentially easterly flow of the order of 20 up to 80 cm s^{-1} in the offshore regions. In near-coastal areas, the direction of flow is modified by the presence of gradient currents set up by sea level rising against the coastline (Fig. 4c). Also, in regions of rapidly changing bottom topography, namely, the area between the Isle of Man and the Cumbrian coast, changes in direction of the surface current are evident, indicating that topographic steering in these regions can extend to the surface current.

Bed currents over the majority of the region exhibit a pressure-driven westerly flow in response to the rise in sea level against the east coast of England. An east–west elevation gradient of the order of 35 cm (Fig. 4c) between the English coast and the model's open boundary occurred in response to this westerly wind.

Surface currents (Fig. 5a) (also at every third grid point of the model) induced by the uniform northerly wind stress, away from coastal influences, show a uniform southerly flow of the order of 30 up to 90 cm s^{-1}, reaching 100 cm s^{-1} at a number of near-coastal points. Again, in regions of rapidly changing bottom topography (for example, the area between the Isle of Man and the Cumbrian coast) some influence of topographic steering is evident. Also, coastal influence upon currents can be seen along the coast of Wales, where water levels have risen (Fig. 5c) in response to the northerly wind.

Bed currents (Fig. 5b) in deep offshore regions (water depths exceeding 40 m) between the Isle of Man and the coast of Anglesey show a northerly pressure-driven flow (of the order of 20 cm s^{-1}) driven by the north–south pressure gradient of order 50 cm (Fig. 5c), which exists between the coasts of Scotland and Wales. However, in shallow near-coastal regions the direct wind-driven forcing dominates, giving rise to a southerly near-coastal flow along the Cumbrian coast and in Liverpool Bay (Fig. 5b). A bottom wind-driven eddy is evident in Liverpool Bay at the junction between the deep water pressure-driven northerly flow and the shallow directly wind-driven southerly flow (Fig. 5b).

Contours of residual wind-induced elevation show a zero contour extending from the open boundary to the south of the Isle of Man then across to the English coast (Fig. 5c). Sea level along the Welsh coast increases by the order of 25 cm, with a similar decrease along the Scottish coast, although in the Solway Firth sea level decreases by over 40 cm (Fig. 5c).

c. *Wind-induced circulation due to uniform westerly and northerly winds with the inclusion of wave–current interaction*

In this section, we examine how the wind-induced circulation, sea surface elevation, and bed friction factor f_c are modified by the inclusion of wave–current interaction. Initially we consider the influence of a wind wave with period of 10 sec and amplitude of 0.5 m, assumed to be in the same direction as the wind stress. Since the level of wave–current interaction depends upon bed roughness z_o and the value of f_c depends upon the reference height z_r [Eq. (17)], then to be consistent with the previous series of calculations, we take $z_r = 100$ cm; hence $k = C_{100} = 0.375 \times 10^{-2}$, giving $f_c = 2k = 0.75 \times 10^{-2}$ and $z_o = 0.146 \times 10^{-2}$ m. A constant wave friction factor $f_w = 0.045$ was used in the calculations.

Since the finite-difference grid in the model is sufficiently fine to resolve the nearshore regions where

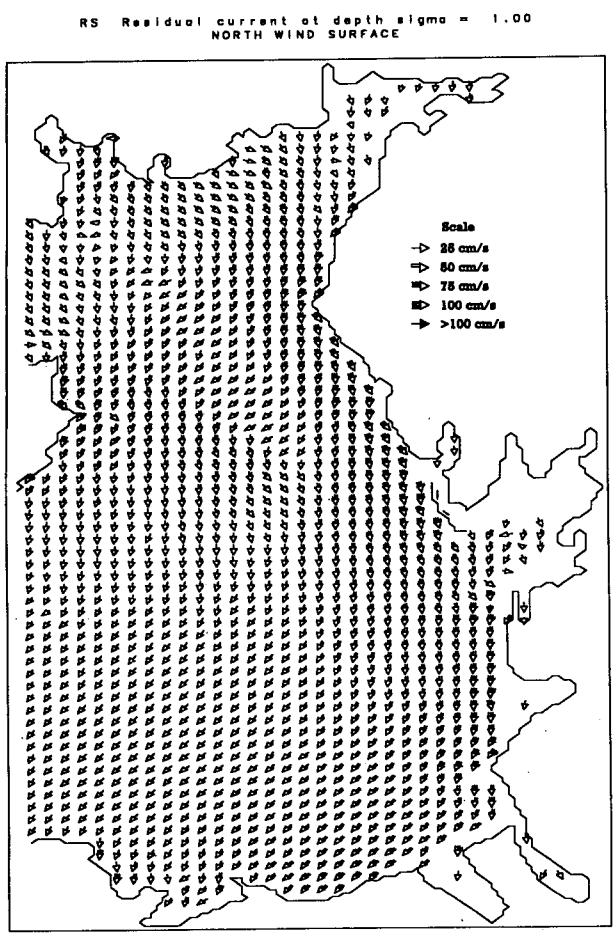

FIG. 5a. Computed surface currents at every third grid point of the model induced by a uniform northerly wind stress of 1 N m^{-2}.

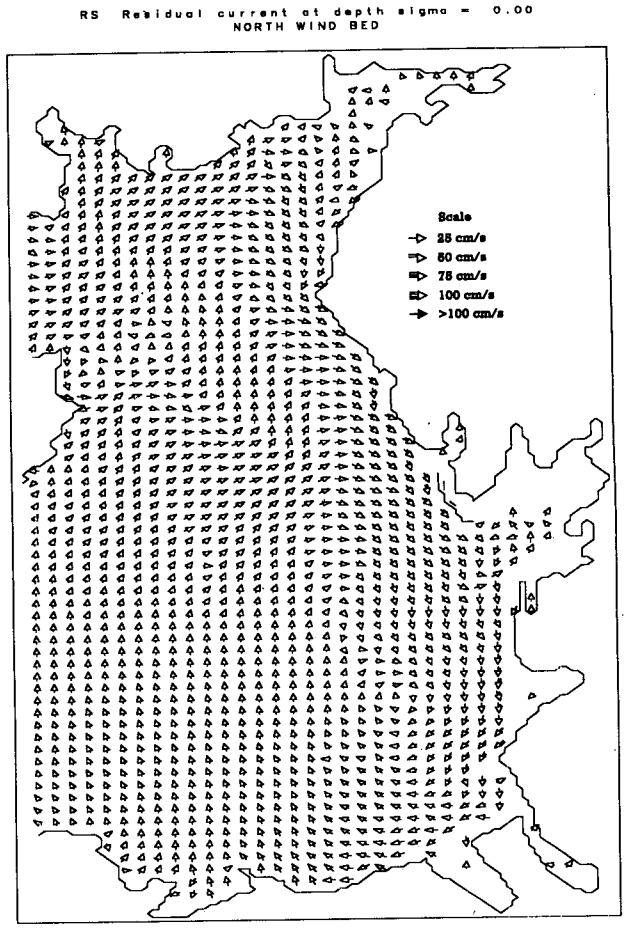

FIG. 5b. As in (a) but for bed currents.

"wetting and drying" occurs at different states of the tide, but not the surf zone, it is necessary to consider how to deal with wave–current interaction in these regions. In shallow water (water depths less than twice the wave amplitude) the wind wave will have broken: Consequently it is physically realistic to assume that the wind wave cannot exist in these regions and, hence, wave–current interaction is not included in these areas.

Surface and bed residual currents computed with wave–current interaction included, induced by the westerly wind stress, show similar circulation patterns to those shown in Figs. 4a,b, although changes in magnitude are evident in shallow water regions. To examine these changes in magnitude in detail, it is instructive to plot the differences between wind-induced residual circulation at surface and bed, with and without wave effects (Fig. 6a,b).

Adding in the effects of waves was found in general to decrease the magnitude of surface and bed currents, particularly in shallow water regions. To examine this effect Figs. 6a,b show a limited area of the model in more detail, namely, the region of Liverpool Bay and the Welsh coast (Fig. 3) where wave–current interaction with the westerly wind was particularly strong. (Wave–current interaction was included over the whole region and did have an effect in other shallow water areas. A detailed plot of the Liverpool Bay area is chosen purely to illustrate the effect.) The change in surface and bed currents can be clearly seen in Figs. 6a,b which is a plot of wind residual with wave–current interaction minus wind residual with no waves. From these figures, it is evident that the strong wind-driven flow from west to east along the Welsh coast is decreased by wave effects. Consequently, taking the difference between wind with waves and wind only produces the flow from east to west shown in Fig. 6a. Similar effects are found in other shallow regions, with changes in current magnitude of order (5–10 cm s^{-1} at the surface, but up to 20 cm s^{-1} in the near bed currents). In deep water regions (water depths exceeding 40 m), wave–current interaction has only a minor effect. In these areas the wave orbital velocity is small of order 10 cm s^{-1} (Table 1), and hence the wave bed stress is small and wave–current interaction is negligible. As stated previously, in very shallow regions the wind wave will have broken

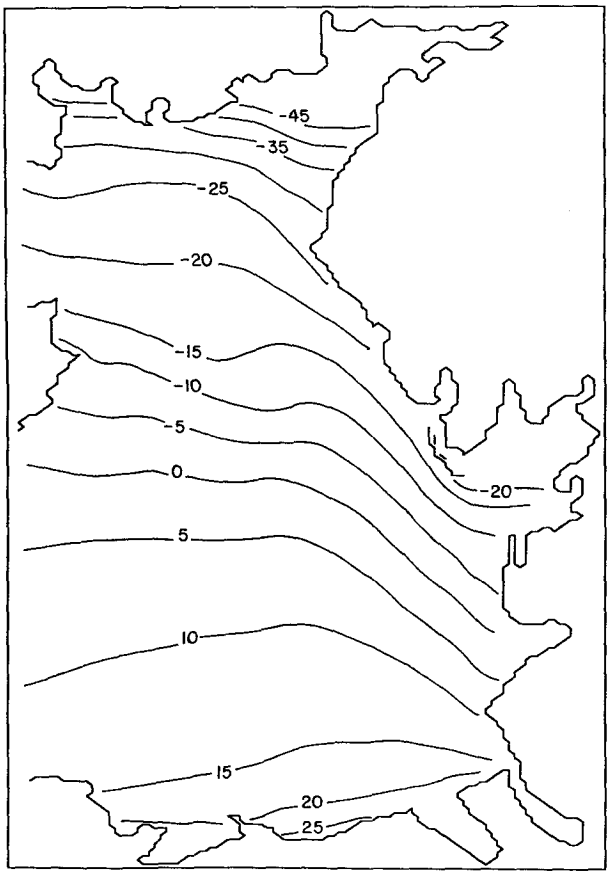

FIG. 5c. Computed residual surface elevation (cm) induced by a uniform northerly wind stress of 1 N m^{-2}.

and wave–current interaction was not included; hence, the near-coastal region with no current vectors in Figs. 6a,b. Although Figs. 6a,b show similar patterns, particularly in shallow water (for example, along the Welsh coast), in deeper water (for example, to the east of the Isle of Man) there are distinct differences.

To understand the decrease in the magnitude of wind-induced flow when wave effects are added and the differences between surface and bed, it is necessary to examine changes in sea surface slope and in the current friction factor f_c when wave–current interaction is included. Changes in sea surface elevation due to enhanced turbulence influencing the bed stress are shown in Fig. 6c. In deep water regions there is a negligible change in sea surface elevation, with changes exceeding 0.5 cm occurring only in the near-coastal area (Fig. 6c).

Contours of the $C_{100} = f_c/2$ (scaled by 10^2), time averaged over a tidal cycle, determined with wave–current interaction included, are shown in Fig. 6d(i). Without wave–current interaction a value of $C_{100} = 0.375 \times 10^{-2}$ would occur over the whole area. Clearly, in the shallow region to the east of the Isle of Man there is a small area [Fig. 6d(i)] where C_{100} exceeds 0.6×10^{-2} (namely, a near doubling of the current friction factor due to wave–current interaction). Similarly, in the near-coastal region, within a narrow area close to the Cumbrian coast, C_{100} exceeds 0.8×10^{-2} associated with the limited shallow water region found here (Fig. 3). A much larger region of enhanced C_{100} [Fig. 6d(i)] occurs in Liverpool Bay, again associated with shallow water (Fig. 3). A significant increase in wave–current friction factor occurs at the entrance to the various estuaries (for example, Solway Firth), although in very shallow water (as explained previously), wave–current interaction was not included.

Contours of the maximum C_{100} value occurring over a tidal cycle are shown in Fig. 6d(ii). Again, the highest C_{100} values occur in shallow near-coastal regions with a large area where C_{100} values exceed 1.0×10^{-2}, occurring to the southwest of Morecambe Bay where water depths are below 20 m. Since the value of f_c, and hence $C_{100} = f_c/2$, depends upon the current bed stress [Eq. (20)], which varies significantly over the tidal cycle in regions such as the eastern Irish Sea, where the flow is rectilinear (Aldridge and Davies 1993), a significant difference between the maximum C_{100} and a time-averaged value [compare Figs. 6d(i) and 6d(ii)] is to be expected.

The reason for the increase of C_{100} in shallow water regions but not deep water due to wave–current interaction can be readily understood from the wave orbital velocity rapid decrease below the surface. Consequently, in deep water (h exceeding 40 m) the wave orbital velocity is small and the influence of wave–current interaction is negligible [Fig. 6d(i) and 6d(ii)]. However, in shallow regions near-bed wave orbital velocity is large (of order 40 cm s^{-1}) and wave–current interaction is large.

The decrease in near-bed current when wave–current interaction is included can also be explained from Fig. 6d(i) in terms of a simple model derived from Eq. (2).

If the influence of the nonlinear terms and rotation are neglected in Eq. (2) and if we integrate from sea surface to seabed, in the steady state $\partial u/\partial t = 0$ and, substituting for F_B, the bed stress (9a) gives

$$\frac{g}{R\cos\phi}\frac{\partial \zeta}{\partial X} = \left[F_s - \frac{f_c}{2}\rho U_h(U_h^2 + V_h^2)^{1/2}\right] \Big/ \rho(h + \zeta). \tag{23}$$

If we assume that the change in $\partial\zeta/\partial X$ due to the addition of wave effects is small (an assumption supported by Fig. 6c), then because the surface stress F_s is specified, any increase in f_c must be accompanied by a decrease in bed currents u_h, v_h if the principal balance in the steady state is between surface and bed stresses.

Changes in the surface current due to enhancements in f_c cannot be so readily explained. From Ekman theory, in the steady state for a constant eddy viscosity

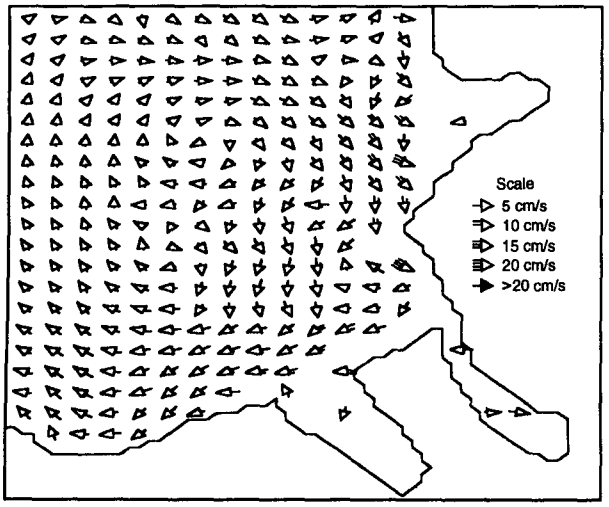

FIG. 6a. Differences between wind-induced surface currents with and without wave–current interaction, computed with a westerly wind stress of 1 N m^{-2}, a wind–wave of amplitude 0.5 m, and period 10 s.

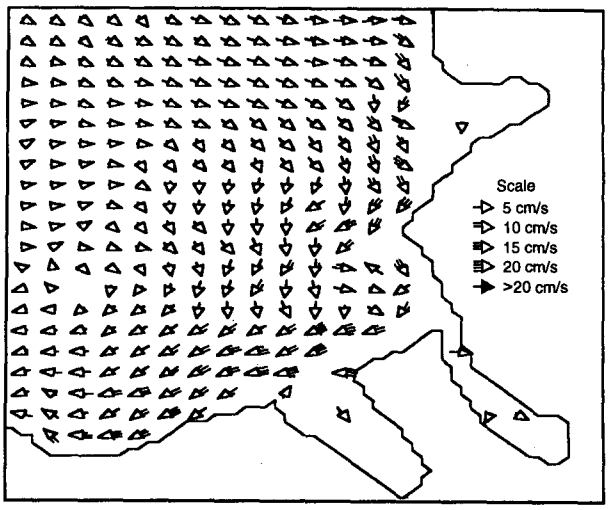

FIG. 6b. As in (a) but for bed currents.

value in an infinitely deep unbounded region, the surface current should be at 45° to the right of the wind [although if the eddy viscosity varies in the vertical (Dyke 1977), a smaller angle occurs]. This is clearly not so in many regions of the eastern Irish Sea (Fig. 4a). In a semienclosed shallow region, however, there are two other important effects, namely, the gradient current due to setup along coastlines (this has clearly occurred here, see Fig. 4c) and the effect of a bottom Ekman layer due to bed stress; both of which cause the surface current to align in a direction other than 45°. Davies (1985) considered the variation in surface current due to changes in bed friction coefficient and found that as the bottom friction coefficient increased, both the surface and bottom currents in shallow water decreased, with the angle between the surface current and the wind falling below 45°.

We now consider the influence of a similar wave field (namely, wave amplitude 0.5 m and period 10 sec, again with f_w fixed at 0.045) upon the wind-induced circulation due to a northerly wind stress. As in the case of the westerly wind, the addition of wave–current interaction does not significantly influence the circulation pattern (Fig. 5a) computed with the northerly wind, although its magnitude changes. In the case of a northerly wind the majority of the wave–current interaction takes place in the shallow water region off the west coast of England. To examine this effect, Figs. 7a,b show a detailed plot of currents in the region to the south of St. Bees Head. (The wave–current interaction did have a significant effect in other shallow water regions, for example, Solway Firth, not shown here.) Differences between the computed flow fields with wave–current interaction and with wind only, at sea surface and seabed, are shown in Figs. 7a,b. In shallow water the flow is driven in the wind's direction and the magnitude of the southward flow that occurs at all depths along the west coast of England is reduced by

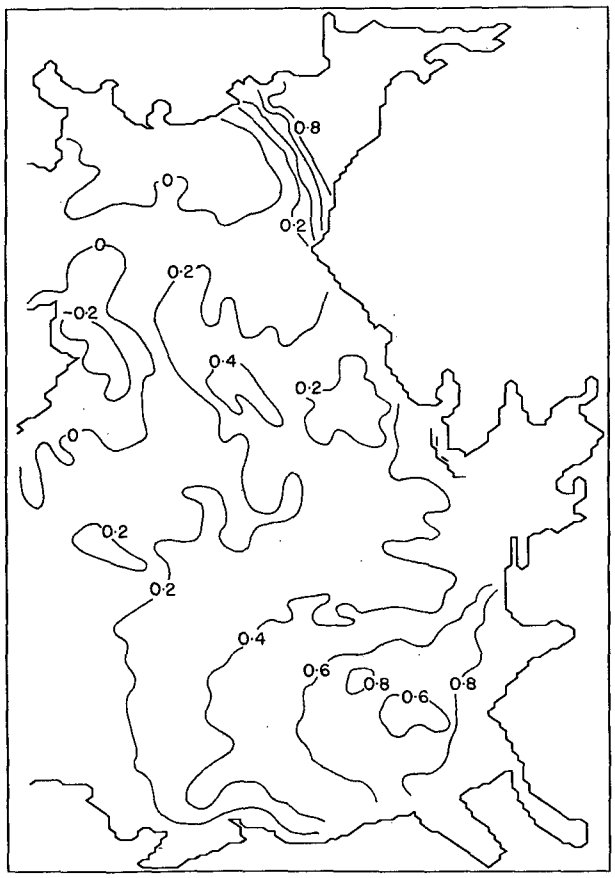

FIG. 6c. Differences between residual sea surface elevation (in cm) with and without wave effects.

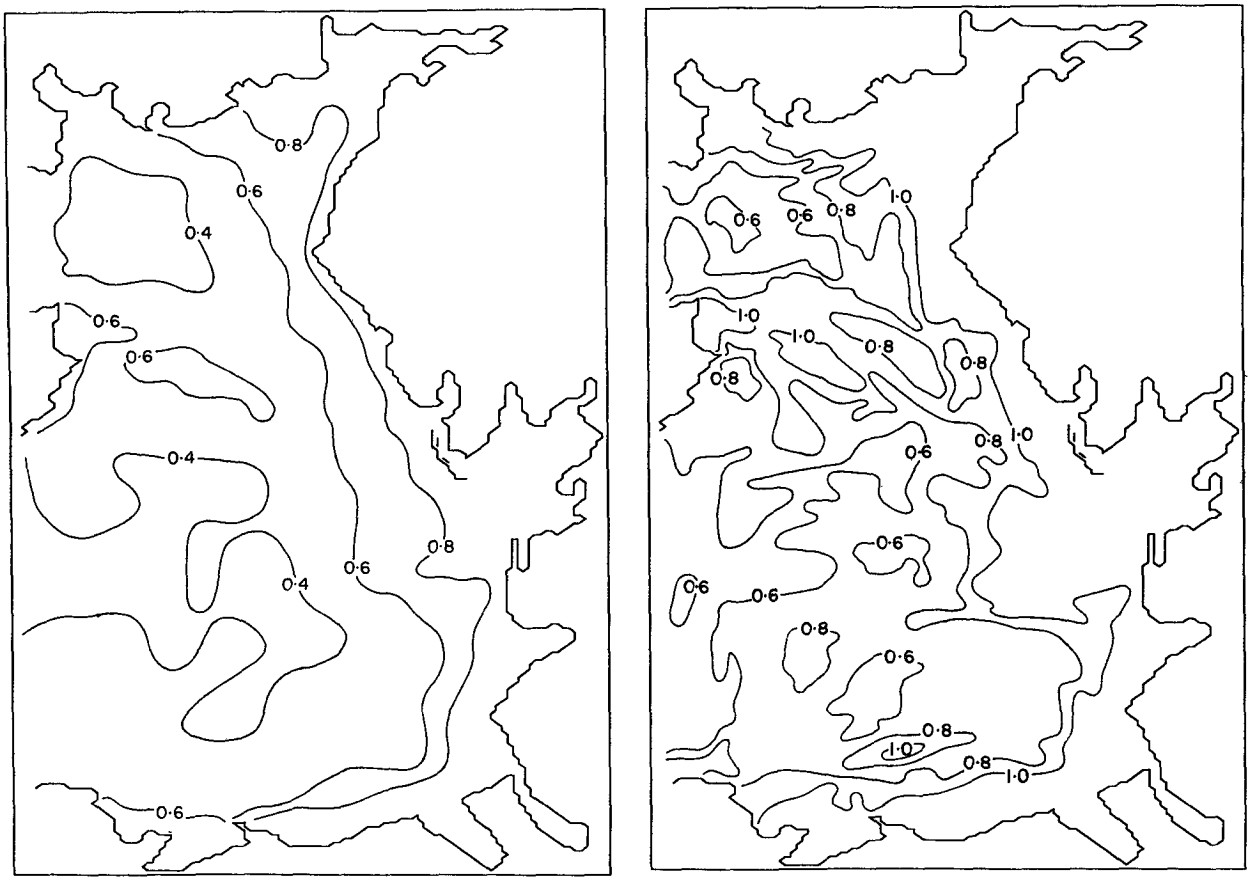

FIG. 6d. Contours of $C_{100} \times 10^2$: (i:left) averaged over a tidal cycle, (ii:right) maximum during a tidal cycle, with wave–current interaction arising from a 10-sec wave period with wave amplitude 0.5 m and a westerly wind stress of 1 N m^{-2}.

the order of up to 5 cm s^{-1} at the surface, with a significantly larger reduction up to 15 cm s^{-1} at the bed (Figs. 7a and 7b). In deeper water the change in current magnitude is much smaller (Fig. 7b), with wind wave effects again producing a decrease in bed currents.

It is interesting to note that the current directions in Figs. 7a,b at the sea surface and sea bed are very similar. At the seabed this corresponds to a decrease in current with the addition of wave effects; similarly, at the sea surface in shallow water the surface current decreases. However, in deep water where the surface current is often in the opposite direction to the bed current, this leads to an increase in surface current. The reason for the decrease in bed currents, with an increase of the surface current in deep water is analogous to that given for westerly winds. As in the case of westerly winds, the change in sea surface elevation is small, only exceeding 1 cm in near-coastal regions.

A similar though not identical spatial distribution in the magnitude (averaged over a tidal cycle) of the drag coefficient C_{100} is found [Fig. 7c(i)] to that arising with the westerly wind (Fig. 6d), with C_{100} increasing significantly in shallow regions. Differences in magnitude of the drag coefficient (Figs. 6d and 7c) arise from differences in the intensity of bed currents (Figs. 4b and 5b) and water depth. As in the previous calculation, the maximum C_{100} value over the tidal cycle (Fig. 7c(ii)] shows a region of C_{100} values exceeding 1.0×10^{-2} in the shallow near-coastal region.

In the previous series of calculations, a wave period of 10 sec was used, initially with a westerly wind and subsequently a northerly wind. To examine the influence of wave period upon the current friction factor and flow field, the calculation was repeated with an identical westerly wind stress and wave amplitude but with a wave period of 6 sec.

As in the previous series of calculations, the influence of wave–current interaction does not significantly affect the general pattern of flow, although bed currents are reduced. Differences between bed currents computed with wave–current interaction and without are shown in Fig. 8a. A similar distribution occurred at the sea surface. (As in the earlier series of calculations, with westerly winds, current vectors are only shown in the Liverpool Bay region for illustrative purposes.)

The spatial variations shown in Fig. 8a are comparable to those in Fig. 6b. The reduction in bed current is, however, significantly less with the 6-sec period wave

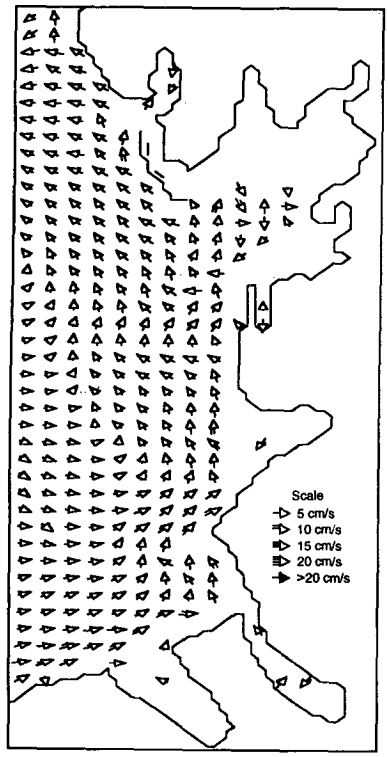

FIG. 7a. As for Fig. 6a but for a northerly wind stress of 1 N m^{-2}.

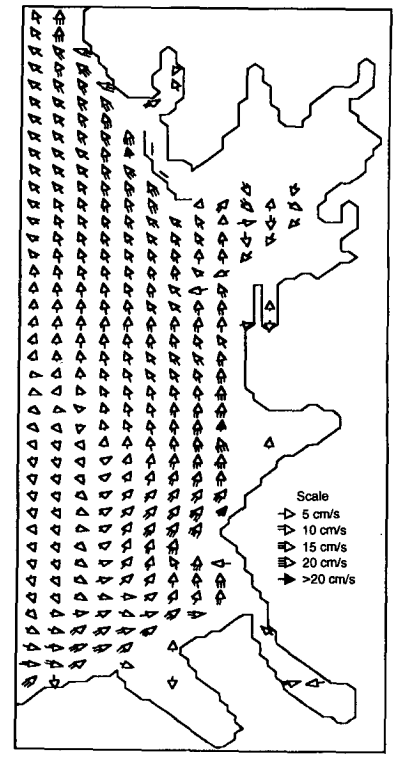

FIG. 7b. As for Fig. 6b but for a northerly wind stress of 1 N m^{-2}.

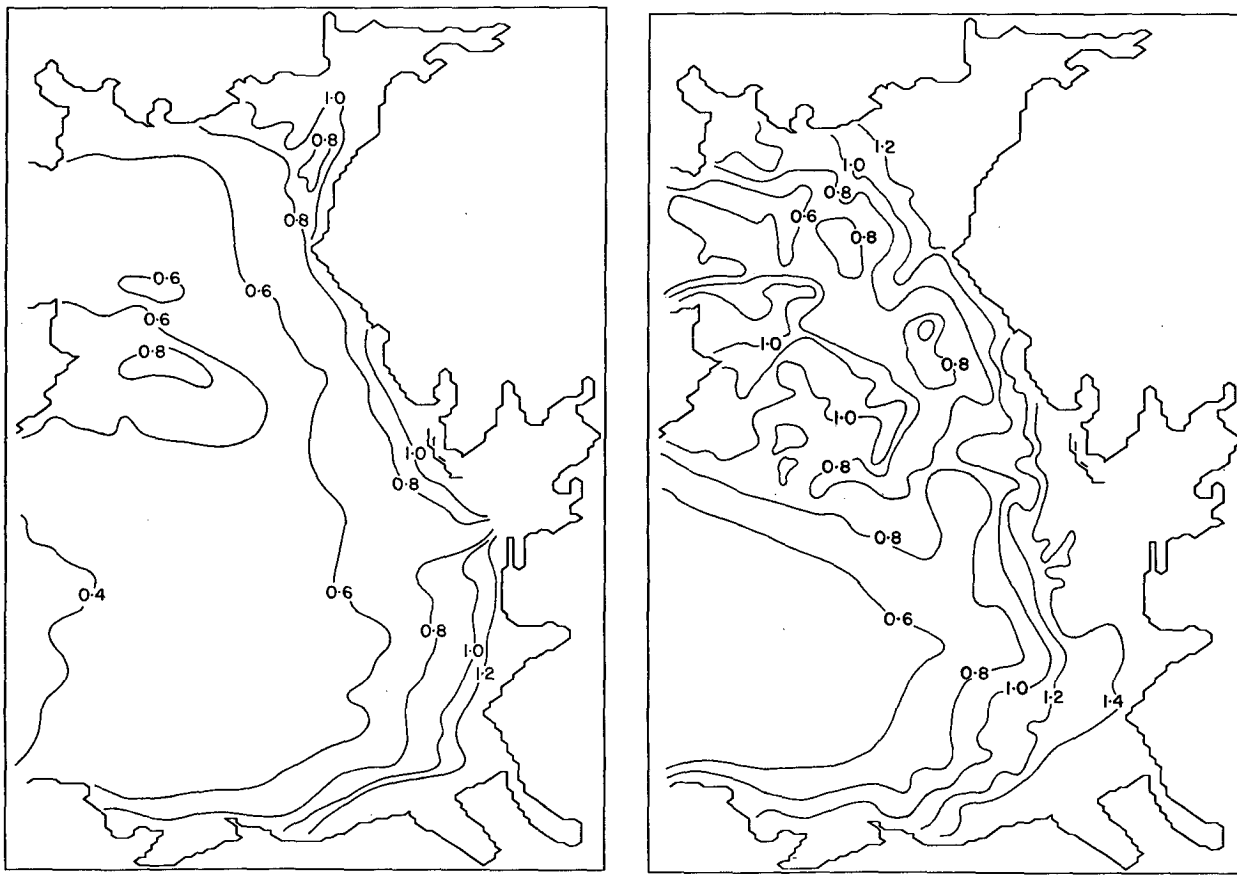

FIG. 7c. As for Fig. 6d but for a northerly wind stress of 1 N m^{-2}.

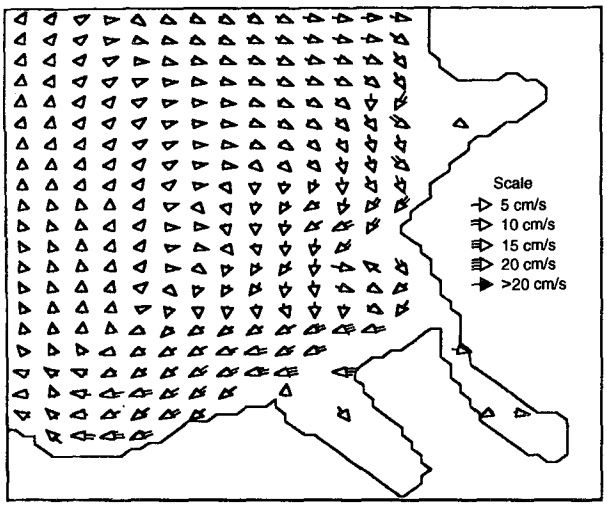

FIG. 8a. Differences between wind-induced bed currents with and without wave–current interaction, computed with a westerly wind stress of 1 N m^{-2}, a wind wave amplitude of 0.5 m, and period of 6 sec.

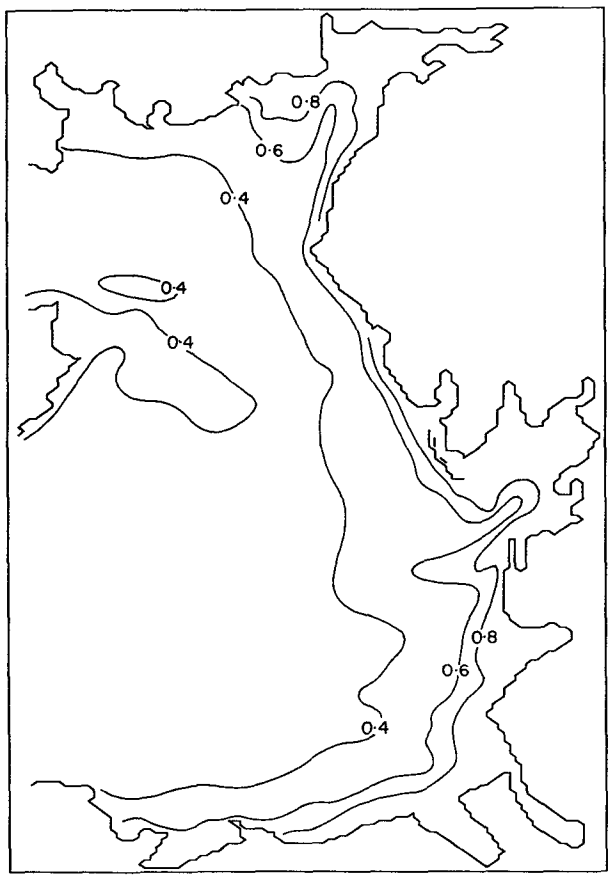

FIG. 8b. Contours of $C_{100} \times 10^2$, averaged over a tidal cycle, with wave–current interaction arising from a 6-sec wave period with amplitude $a_w = 0.5$ m.

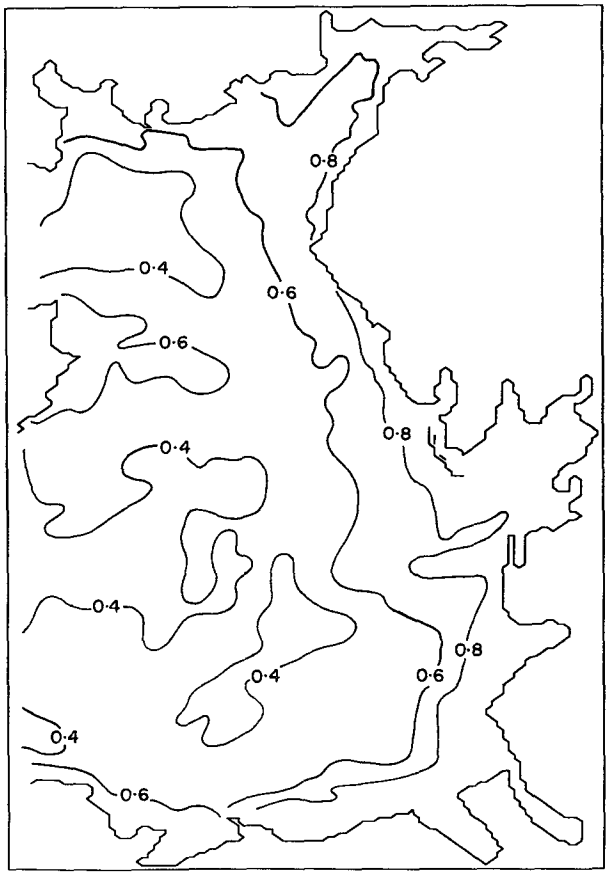

FIG. 9. Contours of $C_{100} \times 10^2$, averaged over a tidal cycle, with wave–current interaction arising from a 10-sec wave period, wave amplitude $a_w = 0.5$ m with a variable bed z_0.

(Fig. 8a) than that found previously with the 10-sec period wave. Also, changes in current are confined to the near-coastal rather than the offshore region. The reason for this can be readily understood in terms of the rate of decay of wave orbital velocity with water depth. A larger rate of decay occurs with a 6-sec period wave than for one of 10-sec period. The reduction in magnitude of the current friction factor (Fig. 8b) compared with that obtained using the 10-sec period wave (Fig. 6d) again is due to the fact that for a given water depth, the near-bed wave orbital velocity of the 6-sec period wave is significantly less than that of the 10-sec period wave.

Similar spatial reductions, although with a smaller magnitude to those found previously, occur with the northerly wind stress with a wave period of 6 sec rather than 10 sec. Also, the spatial distribution and magnitude of the current friction factor computed with a northerly wind and a 6-sec period wave is comparable to that shown in Fig. 8b.

In this series of calculations, a uniform bed roughness $z_0 = 0.146 \times 10^{-2}$ m was used over the whole region. Such an assumption is a significant approximation in

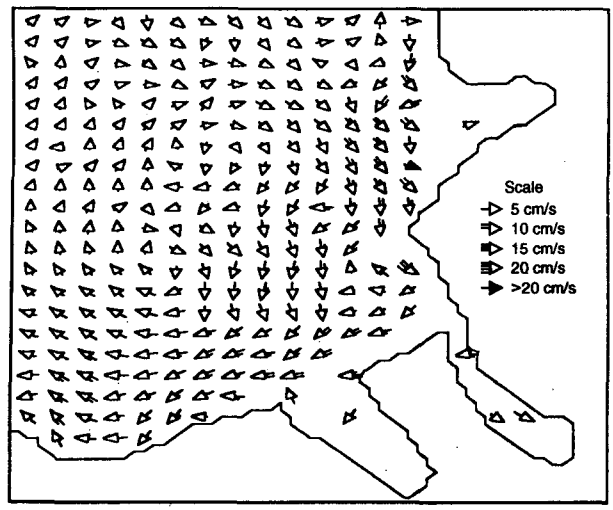

FIG. 10a. Differences between wind-induced surface current with and without wave–current interaction, computed with a westerly wind of 1 N m^{-2}, a wind–wave amplitude of 1.5 m, and a 10-sec period, with a varying z_0 and f_w value.

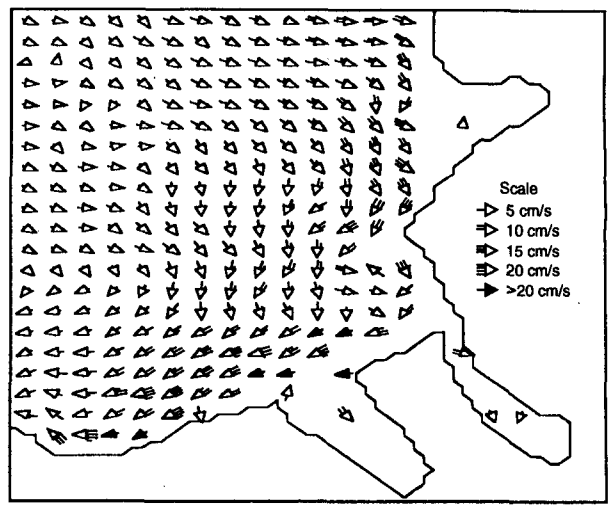

FIG. 10b. As in (a) but for bed currents.

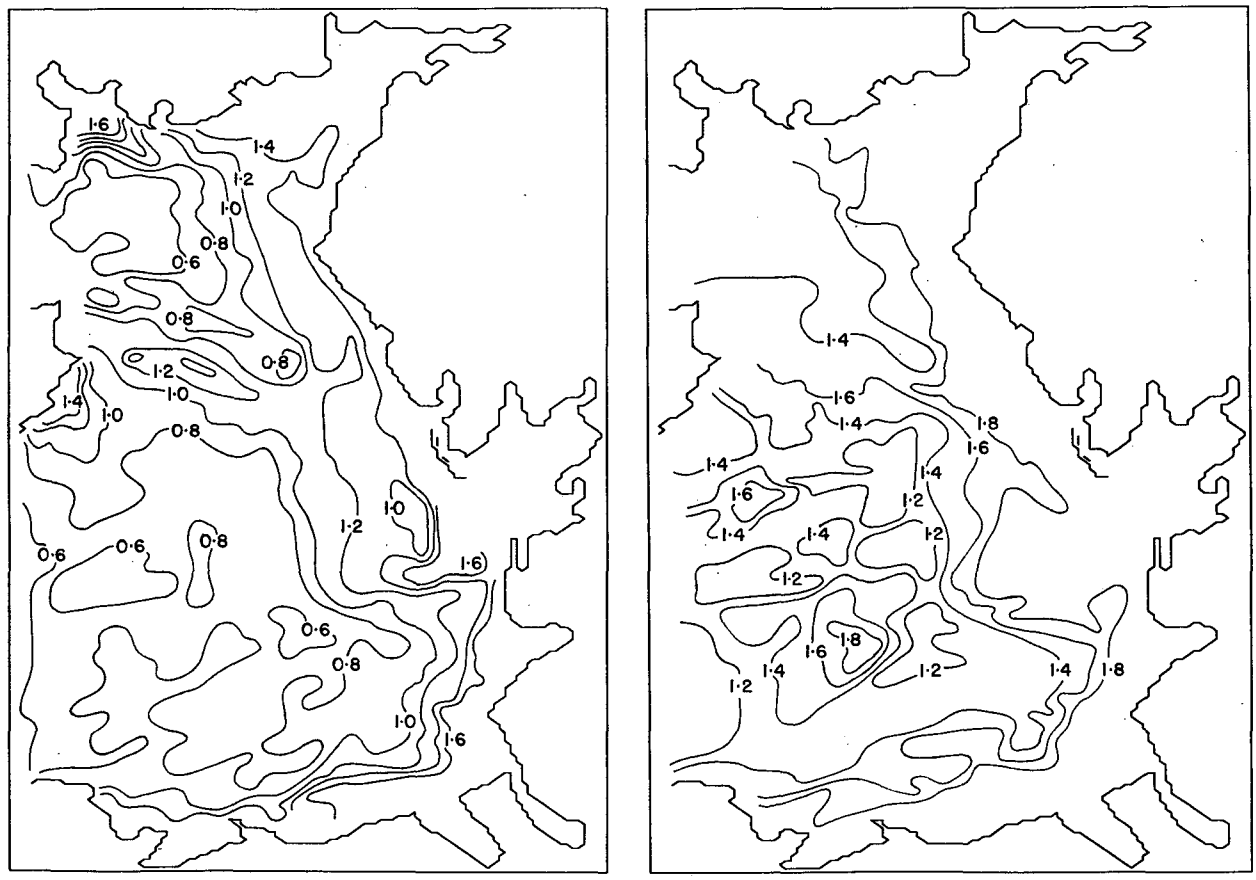

FIG. 10c. Contours of $C_{100} \times 10^2$. (i: left) averaged over a tidal cycle, (ii: right) maximum over a tidal cycle, including wave–current interaction with a wave amplitude a_w = 1.5 m and period T_m = 10 sec, including a varying z_0 and f_w value.

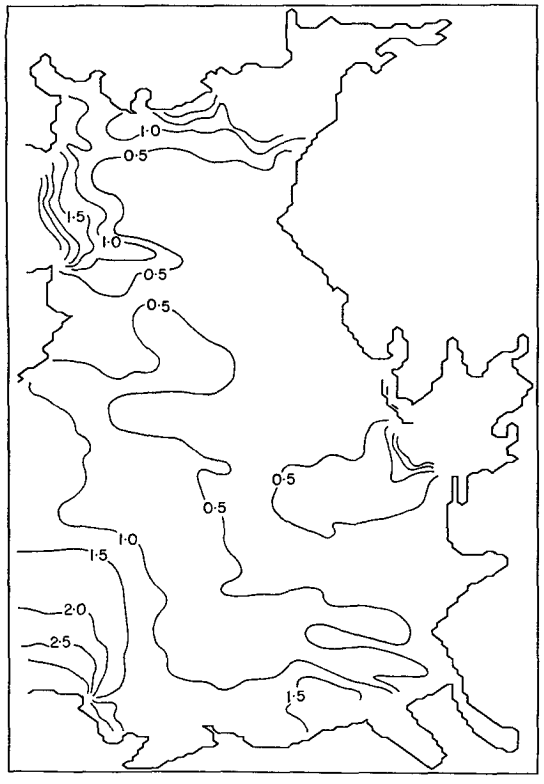

FIG. 11a. Contours of the maximum value of the u component of bed stress (N m^{-2}) computed from the current field.

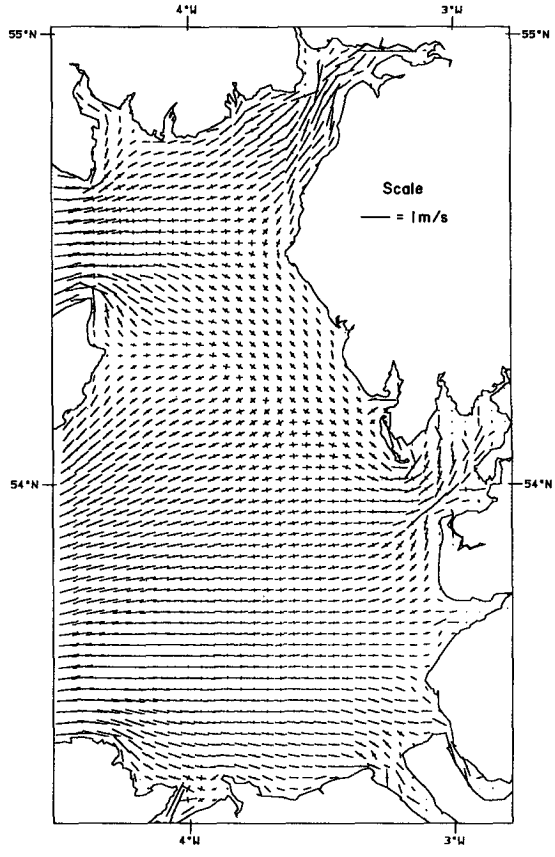

FIG. 11b. Major and minor axis of the M_2 current ellipse at the seabed.

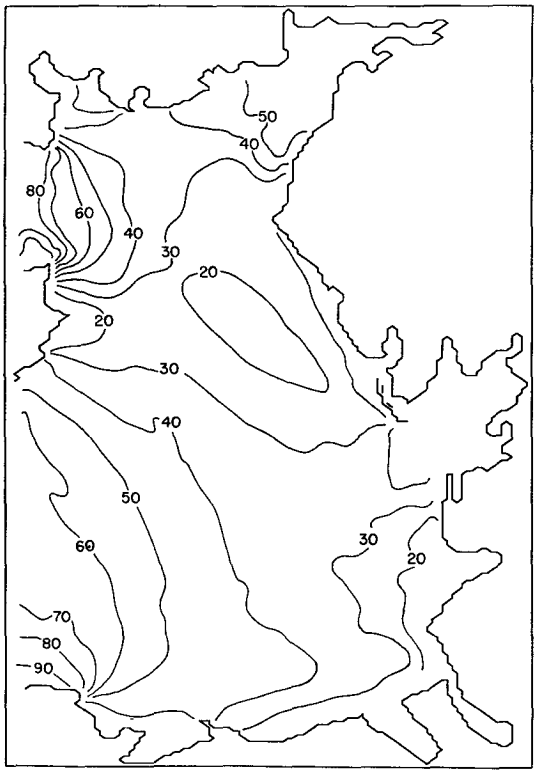

FIG. 11c. Contours of the maximum bed current amplitude (cm s^{-1}) due to tidal and wind-driven flows (westerly wind of 1.0 N m^{-2}).

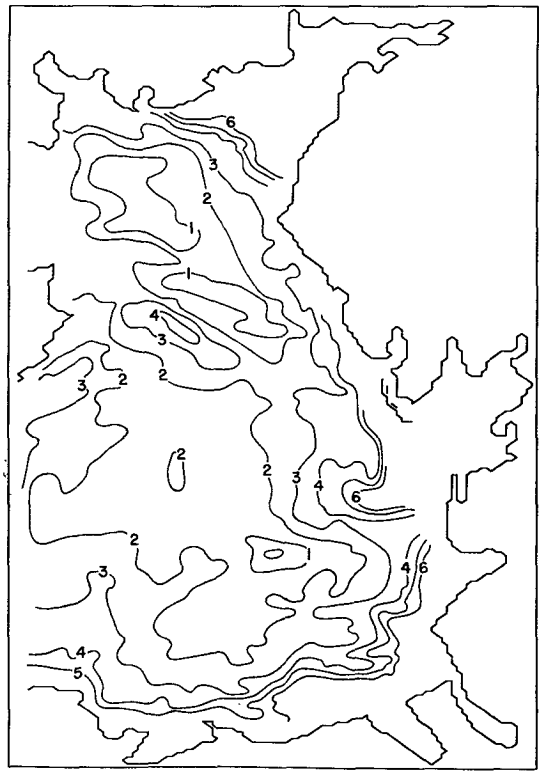

FIG. 11d. Contours of the maximum value of the u component of bed stress (N m^{-2}) due to currents and wind wave orbital velocity (westerly wind stress of 1.0 N m^{-2}, wind waves with a_w = 1.5 m, T_m = 10 s).

that there are major changes in bed types (Fig. 2) and hence values of z_0 over the area. To examine the influence of bed type upon changes in flow field and current friction factor, the series of calculations involving the westerly wind with a 10-sec period wave was repeated, with a spatially varying z_0 reflecting the bed types shown in Fig. 2.

No significant differences (that is, differences below 1 cm s^{-1}) between flow fields determined with a spatially varying z_0 and those shown in Figs. 6a,b were found. Some minor differences in the position of the C_{100} contours [compare Fig. 9, with Fig. 6d(i)] could be detected, thus showing that variations in the bed forms lead to a slightly different distribution of the C_{100} value when taking wave–current interaction into account.

In a final calculation, a spatially varying z_0 was allowed for and the wave friction factor f_w was computed from Eq. (15), giving a physically more realistic set of parameters. To further improve the physical realism of the calculation a wave amplitude of $a_w = 1.5$ m, a physically realistic value during a major wind event, corresponding to a westerly wind stress of 1.0 N m^{-2} was used (Davies and Jones 1992; Carter 1982; Draper 1992).

Differences between the surface and bed wind-induced flow with and without waves are shown in Figs. 10a,b. (As in earlier calculations, only current vectors in the Liverpool Bay region are shown to illustrate the results.) Comparing these with Figs. 6a,b, it is clear that there are slight differences of order 2 cm s^{-1} in the surface flow, although larger differences of order 5 cm s^{-1} are evident in the bed currents, corresponding to a larger reduction in bed current due to the increased wave–current interaction in the present calculation.

Contours of the C_{100} value, both averaged over a tidal cycle [Fig. 10c(i)] and its maximum value [Fig. 10c(ii)], show significantly larger values, both offshore and particularly in the near-coastal region, than those found previously [Fig. 6d(i) and 6d(ii)]. These differences arising primarily due to the larger wave amplitude in the present calculation and that f_w changes over the region.

Since the onset of sediment movement is critically dependent upon whether the bed stress exceeds a threshold value, it is interesting to examine the maximum bed stresses occurring during a tidal cycle. Here we consider the maximum bed stress due to the currents alone (Fig. 11a) and that due to the addition of the current and wave bed stress (Fig. 11d). Since the waves are assumed to be in the current direction, we will consider only the u component of bed stress.

Contours of the maximum u current component of bed stress (Fig. 11a) show regions where the bed stress exceeds 0.5 N m^2, to the north and south of the Isle of Man, corresponding to regions where the tidal currents and tidal plus wind-induced currents are a maximum (Figs. 11b,c), with bed stress increasing rapidly in the Solway Firth. Contours of maximum bed stresses [τ, Eq. (11)] due to a combination of the bed stresses due to the current and that based upon the wave orbital velocity [Eq. (11)] are given in Fig. 11d. It is apparent from this figure that in shallow near-coast regions the maximum bed stress exceeds 5.0 N m^{-2} (an order of magnitude larger than that due to the currents alone). Also, in offshore regions the maximum bed stress is increased by a factor of 4.

5. Concluding remarks

We have developed a three-dimensional hydrodynamic model that can compute tidal and wind-driven currents, including the effect upon them of changes in bed stress due to wave–current interaction. Initial calculations without the influence of wave–current interaction clearly show a significant spatial variation in wind-induced currents in the eastern Irish Sea, even with a uniform wind stress. To first order, surface currents exhibit a fairly uniform flow field, essentially in the wind direction in deep water, although coastal influence and variations in bottom topography do affect the surface currents. Setup along coastlines induces bed currents in the opposite direction to the wind stress. Also, the influence of bottom topography is larger on bed currents than surface currents, producing significantly larger spatial variations in bed currents compared with surface currents.

Enhancements in bed friction coefficient due to wave–current interaction are significant in shallow water with a wave period of 10 sec, diminishing as the wave period is reduced to 6 sec. Increases of the current friction coefficient of the order of factors of 3 are found in the model, and these lead to a reduction in bed currents and changes in surface currents.

Due to the nonlinear nature of the hydrodynamic equations, changes in bed friction coefficient influence both tidal elevations and currents, in particular near-bed currents in the shallow regions resolved with the model. A consequence of this is that the classical approach of computing the wind-induced residual by subtracting a tide-only solution from that involving tide and wind can no longer be applied, and the wind-induced residual had to be computed by performing a harmonic analysis on the total solution. This suggests that it may be difficult to accurately "detide" near-bed current measurements collected during major wind events (with the purpose of studying wave–current interaction) unless a long time series is obtained.

We have only considered a single wind wave amplitude and period, whereas in reality it would be essential to consider a wind wave spectrum and transform this to a characteristic near-bed orbital velocity. Also, in any realistic simulation a wind–wave model would be required to provide the temporal and spatial variation in the wave spectrum. Wave dissipation by bottom friction is particularly important in the near-shore

region, as is the advection and refraction of the wind wave by the near-surface current. These factors suggest that in the future it will be essential to couple three-dimensional circulation and wave models.

The present calculations clearly show that for many sediment transport problems it is essential to consider the influence of wave–current interaction. This is particularly important since during major wind events (when wave heights are large and swell is significant) the total bed stress will exceed its critical value. At this time suspended sediment concentration will increase, and the near-bed currents, the magnitude of which is influenced by wave–current interaction, will be the primary mechanism moving the suspended sediment. Work aimed at addressing these problems is currently in progress, and results will be reported in due course.

Acknowledgments. One author (JL) would like to express his thanks to the director of POL for computing and other facilities during his stay and to MAFF for a year's leave of absence.

The authors are indebted to R. A. Smith for preparing diagrams, and J. Hardcastle for typing the paper.

REFERENCES

Aldridge, J. N., and A. M. Davies, 1993: A high-resolution three-dimensional hydrodynamic tidal model of the eastern Irish Sea. *J. Phys. Oceanogr.*, **23,** 207–224.

Bowden, K. F., L. A. Fairbairn, and P. Hughes, 1959: The distribution of shearing stresses in a tidal current. *Geophys. J. Roy. Astron. Soc.*, **2,** 288–305.

Carter, D. J. T., 1982: Prediction of wave height and period for a constant wind velocity using the JONSWAP results. *Ocean Eng.*, **9,** 17–33.

Christoffersen, J. B., and I. G. Jonsson, 1985: Bed friction and dissipation in a combined current and wave motion. *Ocean Eng.*, **12,** 387–423.

Davies, A. G., 1990: A model of the vertical structure of the wave and current bottom boundary layer. *Modeling Marine Systems,* A. M. Davies, Ed., Vol. 2, CRC Press, 263–297.

——, 1991: Transient effects in wave–current boundary layer flow. *Ocean Eng.*, **18,** 75–100.

——, R. L. Soulsby, and H. L. King, 1988: A numerical model of the combined wave and current bottom boundary layer. *J. Geophys. Res.*, **93,** 491–508.

Davies, A. M., 1983: Formulation of a linear three-dimensional hydrodynamic sea model using a Galerkin-Eigenfunction method. *Int. J. Num. Meth. Fluids,* **3,** 33–60.

——, 1985: A three-dimensional modal model of wind induced flow in a sea region. *Progr. Oceanogr.*, **15,** 71–128.

——, 1986: A three-dimensional model of the north west European Continental Shelf, with application to the M_4 tide. *J. Phys. Oceanogr.*, **16,** 797–813.

——, 1987: Spectral models in Continental Shelf Sea Oceanography. *Three-Dimensional Coastal Ocean Models,* N. S. Heaps Ed., Amer. Geophys. Union, 71–106.

——, 1992: Modelling currents in highly sheared surface and bed boundary layers. *Contin. Shelf Res.*, **12,** 189–211.

——, and J. E. Jones, 1990: Application of a three dimensional turbulence energy model to the determination of tidal currents on the Northwest European Continental shelf. *J. Geophys. Res.*, **95,** 18 143–18 162.

——, and J. N. Aldridge, 1992: A stable algorithm for bed friction in three dimensional shallow sea modal models. *Int. J. Num. Meth. Fluids,* **14,** 477–493.

——, and J. E. Jones, 1992: A three dimensional wind driven circulation model of the Celtic and Irish Seas. *Contin. Shelf Res.*, **12,** 159–188.

——, R. B. Grzonka, and M. O'Neill, 1991: Development and application of 3D shallow sea models on the CRAY computer. *Science and Engineering on Cray Supercomputers,* E. J. Pitcher, Ed., Computational Mechanics Publications, Springer Verlag, 323–334.

——, ——, and C. V. Stephens, 1992: Implementation of a three-dimensional hydrodynamic numerical sea model using parallel processing on a Cray X-MP Series computer. *Advances in Parallel Computing,* Vol. 2, D. J. Evans, Ed., JAI Press, 145–185.

Draper, L., 1992: *Wave Climate of the British Isles.* HMSO OTH 89 303, 1–36. [ISBN 011 4130 92 2.]

Dyke, P. P. G. 1977: A simple ocean surface layer model. *Riv. Ital. Geofis.*, **4,** 31–34.

Flather, R. A., and N. S. Heaps, 1975: Tidal computations for Morecambe Bay. *Geophys. J. Roy. Astron. Soc.*, **42,** 489.

——, and K. P. Hubbert, 1990: Tide and surge models for shallow water—Morecambe Bay revisited. *Modeling Marine Systems,* Vol 1, A. M. Davies, Ed., CRC Press, 135–166.

Furnes, G. K., 1983: A three dimensional numerical sea model with eddy viscosity varying piecewise linearly in the vertical. *Contin. Shelf Res.*, **2,** 231–242.

Gordon, R. B. and M. L. Spaulding, 1987: Numerical simulations of the tidal- and wind-driven circulation in Narragansett Bay. *Estuarine, Coastal Shelf Sci.*, **24,** 611–636.

Grant, W. D., and O. S. Madsen, 1979: Combined wave and current interaction with a rough bottom. *J. Geophys. Res. (Oceans),* **84,** 1797–1808.

——, A. J. Williams, and S. M. Glenn, 1984: Bottom stress estimates and their prediction on the Northern California Continental Shelf during CODE-1: The importance of wave–current interaction. *J. Phys. Oceanogr.* **14,** 506–527.

Green, M. O., J. M. Rees, and N. D. Pearson, 1990: Evidence for the influence of wave–current interaction in a tidal boundary layer. *J. Geophys. Res.*, **95,** 9629–9644.

Huntley, D. A., and A. J. Bowen, 1990: Modeling sand transport on continental shelves. *Modeling Marine Systems,* A. M. Davies, Ed., CRC Press, 221–254.

James, I. D. 1990: Numerical modelling of density-driven circulation in shelf seas. *Modeling Marine Systems,* Vol. 2, A. M. Davies, Ed., CRC Press.

Jonsson, I. G. 1967: Wave boundary layers and friction factors. *Proc. 10th Int. Conf. on Coastal Engineering 1966,* New York, NY, Amer. Soc. Civ. Eng. 127–148.

——, and N. A. Carlsen, 1976: Experimental and theoretical investigations in an oscillatory turbulent boundary layer. *J. Hydraul. Res.*, **14,** 45–60.

Lohrmann, A., B. Hackett, and L. P. Roed, 1990: High-resolution measurements of turbulence, velocity, and stress using a pulse to pulse coherent sonar. *J. Atmos. Oceanic Technol.*, **7,** 19–37.

Oey, L.-Y., G. L. Mellor, and R. I. Hires, 1985: A three-dimensional simulation of the Hudson–Raritan estuary. Part 1: Description of the model and model simulations. *J. Phys. Oceanogr.*, **15,** 1676–1692.

Signell, R. P., R. C. Beardsley, H. C. Graber, and A. Capotondi, 1990: Effect of wave–current interaction on wind-driven circulation in narrow, shallow embayments. *J. Geophys. Res.*, **95,** 9671–9678.

Spaulding, M. L., and T. Isaji, 1987: Three dimensional continental shelf hydrodynamic model including wave current interaction. *Three-Dimensional Models of Marine and Estuarine Dynamics.* J. C. J. Nihoul and B. M. Jamart, Eds., Elsevier, 405–426.